Tubular Anti-resonant Hollow Core Fiber for Visible Raman Spectroscopy

Ian A. Davidson*, Matthew Partridge, John R. Hayes, Yong Chen, Thomas D. Bradley, Hesham Sakr, Shuichiro Rikimi, Gregory T. Jasion, Eric Numkam Fokoua, Marco Petrovich, Francesco Poletti, David J. Richardson and Natalie V. Wheeler

Optoelectronics Research Centre, University of Southampton, Southampton, SO17 1BJ, U.K.

Abstract

We report low loss, wide bandwidth, tubular anti-resonant hollow core fibers with a low macro- and micro- bend sensitivity tailored for gas sensing using visible wavelength Raman spectroscopy. The fibers show record low bend sensitivity for anti-resonant fibers operating in this spectral region. A minimum loss of 23.6 dB/km is measured at 570nm for a fiber spooled on a 30cm diameter drum.

Keywords: hollow core fibers, microstructured fibers, Raman spectroscopy, gas sensing

*I.A.K.Davidson@soton.ac.uk

I Introduction

Hollow core fibers (HCFs) have been extensively investigated for use in gas detection via various techniques in applications ranging from environmental and industrial process monitoring to early stage disease detection through breath analysis [1,2]. As gas can be loaded into the hollow core region of HCFs and interact with the light guided there over very long path lengths (determined only by the fiber's length or attenuation) HCFs can provide enhanced sensitivity. Optical gas detection through Raman spectroscopy is a very promising gas detection technique allowing simultaneous detection of multiple gas species, as Raman scattering from the molecules in a gas sample produces a spectrum with distinct features which can be directly correlated to the gas composition. While Raman scattering in gas is very weak, this can be overcome by the long path length provided by a HCF, enabling high sensitivity gas detection, as well as multi-species identification. So far, the lowest limit of detection reported is 0.2 ppm for methane gas [3].

In most published work on Raman sensing using HCF, the fiber used was a hollow core photonic bandgap fiber (HC-PBGF) along with a visible wavelength pump laser, as the Raman scattering co-efficient scales with λ^{-4}. However, in this spectral region, HC-PBGFs have three key drawbacks for Raman gas sensing applications: firstly, the core size is typically very small (~5 µm [4]) which limits how quickly the fiber can be filled with gas; secondly, HC-PBGF attenuation scales with λ^{-3} [5] and thirdly, the fiber's low loss bandwidth is usually limited to ~50 nm in the visible [4], limiting the range of Raman signals (and hence gas species) which can be simultaneously detected.

Recently, anti-resonant HCFs (AR-HCFs) have emerged as true competitors to HC-PBGFs for many applications. In 2018 an AR-HCF with a record low loss for any HCF design was reported (1.3 dB/km at 1450 nm [6]). As well as reduced attenuation, AR-HCFs can provide wider operating bandwidths and larger core diameters than HC-PBGFs. Possible drawbacks include higher bend sensitivity and lower Raman capture efficiency. Currently, state-of-the-art visible-guiding AR-HCFs have demonstrated low attenuation (13.8 dB/km at 539 nm [7]) but these fibers are more bend sensitive than the fibers described here, which could limit their suitability for practical deployment. Gao et al. [8], have reported a "conjoined tube" fiber, where each tubular unit consists of two tubes joined together resulting in fiber with a very low loss of 3.8dB/km at 680nm, showing that the low loses demonstrated in these more structurally complex fibers can scale to the visible wavelength range.

Here, we report the fabrication and characterization of two tubular AR-HCFs, designed for Raman sensing, which rival the optical properties of state-of-the-art tubular fibers, when considering attenuation, macro- and micro- bend loss, moving these fibers closer to deployment in practical devices.

II Fiber Design, Fabrication and Characterization

1. Fiber Design and Fabrication

For this work we chose to use a 7 element tubular HC-ARF as modelling indicates this is the best compromise between loss, macro-bend loss, and higher order mode suppression [9] for this fiber type. We also chose to limit the core diameter to around 20 µm, as this appears to be a good balance between overall attenuation (limited by confinement loss, which decreases with core size) and bend sensitivity (which increases with core size, for a given wavelength). Furthermore, this core size is substantially larger than that of a visible wavelength HC-PBGF, enabling faster gas filling times [10]. For the Raman sensing application, we use a 532nm pump laser. The largest Raman shift we aim to detect is for the vibrational hydrogen Stokes line, which, for this pump wavelength, is at 683nm. Hence, we chose to design our fiber to operate in the second anti-resonant transmission window in order to provide the required bandwidth, without the complexity of targeting fundamental window operation, which for visible wavelengths requires very thin glass membranes and that represents a far harder fabrication challenge.

The two fibers reported here were fabricated in a multi-stage process. Hereaus F300 tubes were initially drawn into a series of uniform capillaries. These were then stacked and fused into an initial preform with a diameter ~ 2cm. This stack was then drawn into millimeter-scale canes, and these canes jacketed to make a final fiber preform. During fiber drawing a multi-zone pressurization system was used to control the fibers' final structure [11]. Both fibers were drawn from nominally identical canes, with only the dimensions of the jacket tube (and hence fiber glass outer diameter, OD) changing.

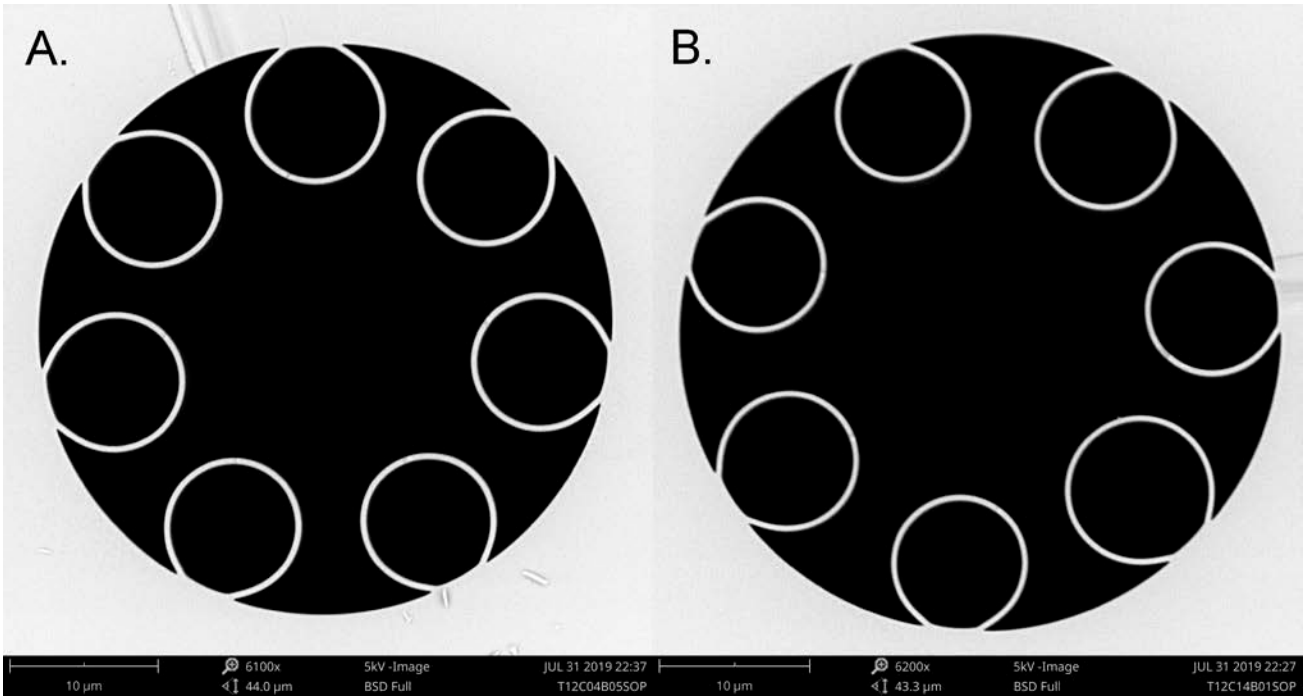

Figure. 1 SEM images of fibers A and B

Table I: Key structural and optical parameters of fibers A and B (reported here) compared to state-of-the-art tubular fibers from the literature [7, 12].

	Fiber A	Fiber B	Fiber C [7]	Fiber D [12]
Minimum Loss (wavelength)	35.9 dB/km (619nm)	23.6 dB/km (570nm)	13.8 dB/km (539nm)	80 dB/km (532nm)
Loss at 532nm	65.7 dB/km	26.0 dB/km	~ 17 dB/km	80 dB/km
3dB bandwidth	62nm	71nm	~40nm	~45nm
Macro-bend loss (16cm bend diameter, 532nm)	0.1dB/m	0.12dB/m	~1.4 dB/m (at 15cm diameter)	0.2 dB/m
Core diameter (μm)	20.5±0.2	20.6±0.1	41	26
Cladding tube gap (μm)	3.5 ± 0.4	3.8±0.6	2.2 - 4	7
Membrane thickness (nm)	440 ± 10	428±30	610	210
Fiber outer diameter (μm)	140	223	Not Available in Literature	200

2. Fiber Characterization

(1) Structural Characterization

The physical dimensions of fibers A and B were measured from scanning electron micrograph (SEM) images (see Figure 1) taken using a Phenom ProX desktop SEM system. The key structural parameters are detailed in Table I. As expected the features of the microstructure are very similar (as the fibers are from similar canes). One small difference is that the membrane thicknesses in fiber B are slightly thinner, which results in the transmission window shifting to shorter wavelengths.

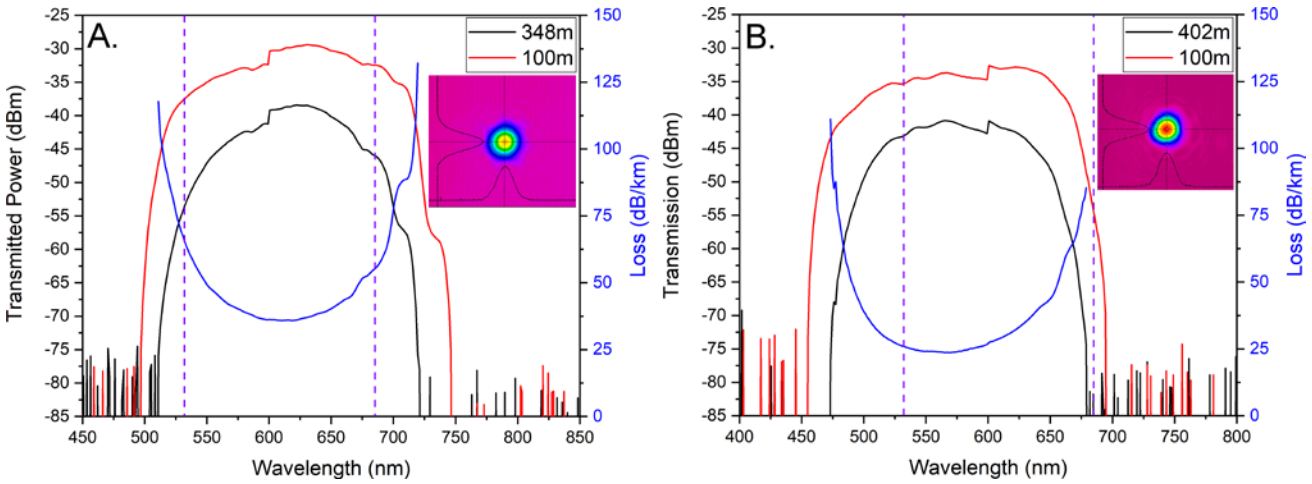

Figure 2. The transmission (red and black curves) and loss (blue curves) are shown for fiber A and B respectively, purple lines have been added to show the 532 and 683nm wavelengths as a guide to the eye. The obvious step feature at 600nm is due to the OSA switching gratings at that wavelength. Inset are beam profile images.

(2) Transmission and Loss Measurements

The fibers' transmission and loss (Figure 2) were characterized using a NKT SuperK COMPACT super-continuum laser system and a Yokogawa AQ-6315A optical spectrum analyzer (OSA) using an SMF28 launch fiber. As expected, the

transmission window of fiber B is shifted ~40nm towards shorter wavelengths. Fiber attenuation was measured using the cutback technique; fibers A and B were cut from 348m and 402m respectively to 100m, to ensure the modal content was consistent between both lengths and to enable comparison between the two measurements. During the measurements the fibers were spooled on ~30cm diameter bobbins under 20g of tension. The key loss values for both fibers are summarized in Table I.

The beam profile images inset in Figure 2 were recorded using a silicon CCD camera (Spiricon Scorpion, SCOR 20) and aspheric collimating lens (Thorlabs C260TME). The fibers were illuminated with a 632.8nm HeNe laser (Melles Griot 05-LHR-151-181), which was directly launched into the core of the HCF using another aspheric lens (Thorlabs C260TME).

The low-loss bandwidth of these fibers is essential for their use in Raman spectroscopic gas measurements as it enables the simultaneous detection of multiple species that is a key feature of this technique. An example of this is shown in Figure 3, where a 10m length of fiber A was filled with 3 bar of 3% hydrogen in nitrogen gas, and then pumped with 145mW, and clearly shows the vibrational Raman emission (1st Stokes) lines of both the nitrogen (at 2330cm^{-1}) and hydrogen (at 4160cm^{-1}), along with some trace oxygen (580nm/1556cm^{-1}) and water vapor (OH$^-$ at 660nm/3645cm^{-1}).

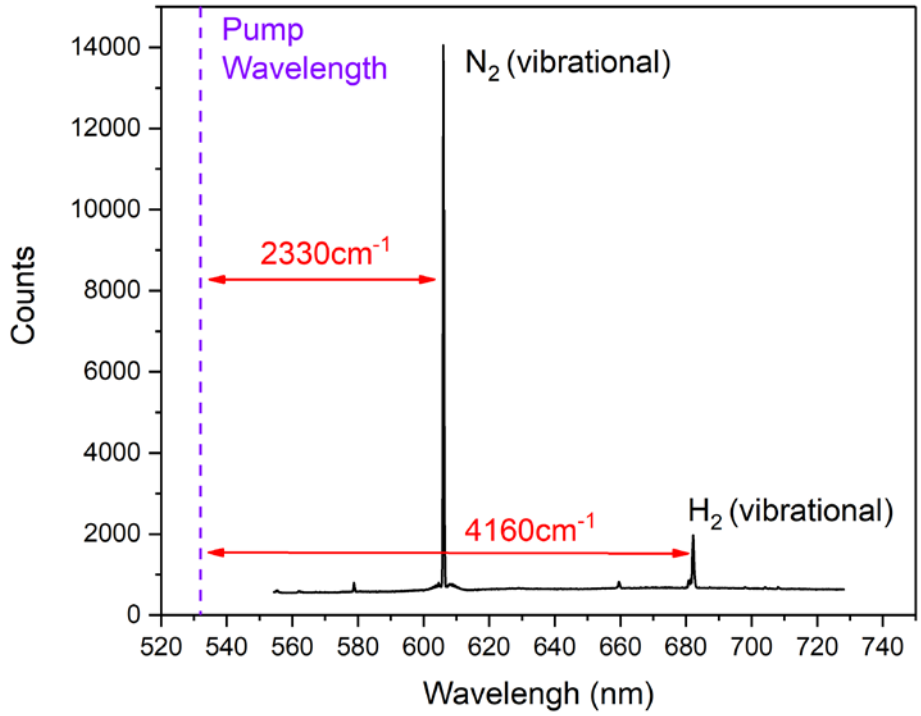

Figure 3. Results of a Raman measurements made with fiber A showing the nitrogen and hydrogen vibrational Raman emission (1st Stokes) lines at ~2330cm^{-1} (N_2) and 4160cm^{-1} (H_2).

(3) Macro-bend Measurements

Macro-bend measurements were made using a series of precision inscribed grooves in an acrylic plate. Light from a halogen lamp was launched into the fiber using an SMF28 patch cable mounted on a micro-positioning stage. The transmitted power was measured using the same OSA as above. As the fiber length used was only ~4m, and the modal content of the fiber was not directly measured, the reported bend-losses represent the worst case scenario, as higher order modes are expected to be more bend-loss sensitive than the fundamental.

The results of the macro-bend measurements are shown in Figure 4 at 532nm and 683nm, the extremes of our desired operating wavelength range. The results show that down to bend diameters of 13cm, fibers A and B show very low bend sensitivity. Furthermore, in Figure 4, the macro-bend performance of two state-of-the-art tubular ARFs from the literature, fibers C and D [7, 12] are also shown. Comparing fibers A and B with these state-of-the-art fibers, shows that fibers A and B demonstrate much lower bend sensitivity.

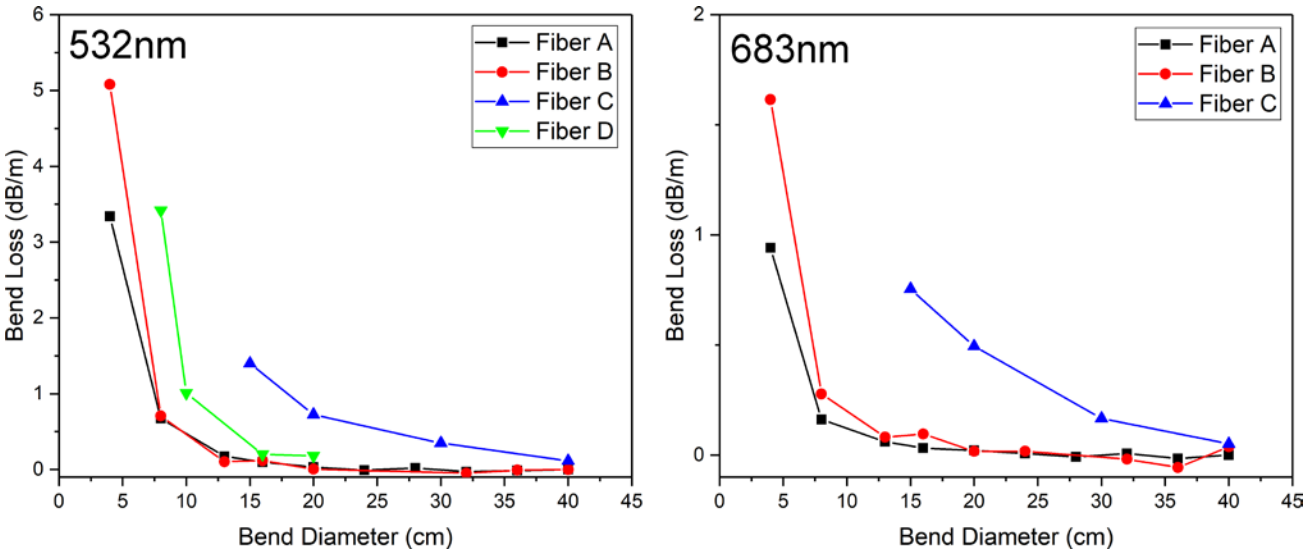

Figure 4. Macro-bend loss vs. bend diameter for fibers A-D. The data for fibers C and D were taken from ref. [7] and [12].

(4) Micro-bend Measurements

Micro-bend sensitivity is another important fiber loss mechanism, and relates to losses induced by subjecting a fiber to millimeter and sub-millimeter lengths scale bends. The dynamics of this mechanism are different to those of traditional macro-bending (induced by centimeter or larger length scale bends) and hence this needs to be evaluated separately [13]. It can become a factor when a fiber is being deployed in a non-ideal environment, outside the lab for example, where the fiber may end up pressed against a rough surface or point strains may induces localized fiber distortions.

Micro-bend measurements were made using a purpose built system with structural perturbations at a fixed spatial frequency over which fibers can be tensioned. Set amounts of stress were applied to 100m of each fiber (in roughly 25MPa steps) and the transmission through the fiber measured at each step. The transmission set-up used for these measurements was identical to that used for the cutback measurements. The results for both fibers are shown in Figure 5.

As can clearly be seen in these measurements, fiber B is substantially less sensitive to micro-bend, as it is necessary to apply nearly 50MPa of fiber stress (200g of tension) before any transmission degradation is seen, whereas the transmission of fiber A starts to degrade when even minimal amounts of fiber stress/ tension are applied. This effect is further magnified as the smaller glass dimension of fiber A (compared to B) mean even a minimal tension (of the order of 10-20g) is sufficient for performance degradation to occur.

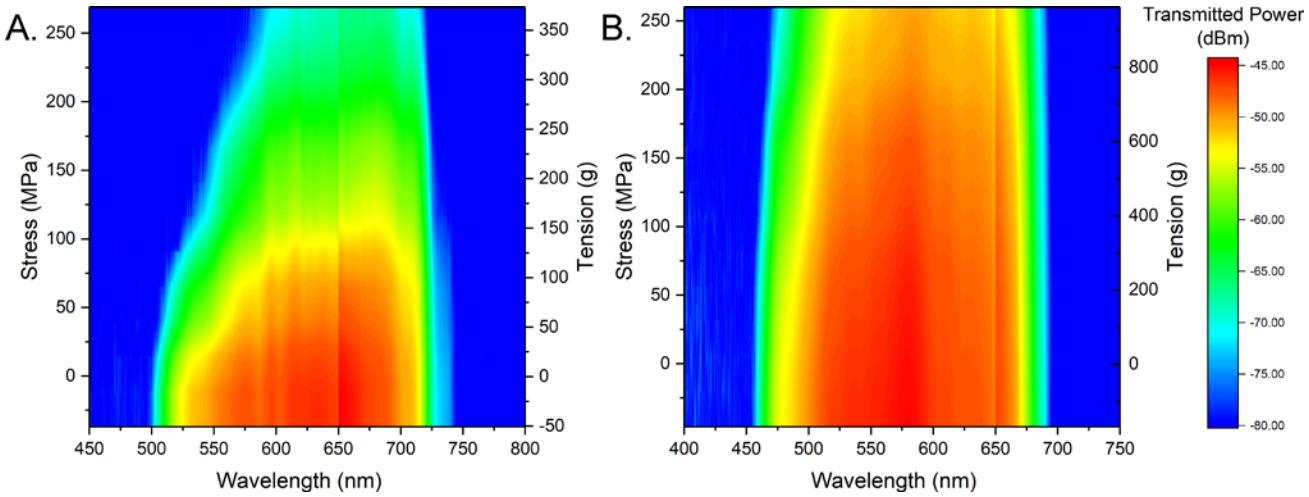

Figure 5. Micro-bend measurements of Fiber A (left) and Fiber B (right). The linear feature at 650nm is due to the OSA switching gratings at that wavelength for this measurement range.

Although the fibers reported here perform well, it is likely further improvements can be made in terms of loss without compromising their low bend sensitivity through design and fabrication optimization. This is an area that to explore in future through efforts to further optimize the combination of core diameter, tubular element gaps and size, and fiber OD, to see how far we can push this technology. Ultimately, the introduction of nested elements (an additional tube within the existing tubular elements) during fabrication seems a more complete solution to the problem of realizing low loss fibers with excellent bend-loss performance, albeit at the expense of greater fabrication complexity [6,8,14].

IV Conclusions

We report on work towards realizing practical, low loss, wide bandwidth HC-ARFs with reduced bend sensitivity for the visible spectral window. Two fibers are reported, A and B, which have minimum losses of 35.9dB/km and 23.6dB/km respectively and exhibit record low bend sensitivity for visible-guiding tubular AR-HCF. This performance makes these fibers highly attractive for a wide range of applications, including Raman spectroscopy. As structurally the key difference between the two fibers is the glass cladding thickness, the micro-bend performance has been characterized and it was found that, due to the thicker cladding of fiber B, its micro-bend sensitivity is substantially reduced; this likely also accounts for the difference in the two fibers overall attenuation. Apart from demonstrating progress in HCF fabrication at these wavelengths, these results also demonstrate the need for thorough HCF characterization beyond simple attenuation measurements (when in a loosely spooled condition) to fully assess their suitability for deployment in practical devices, which is very timely considering recent breakthroughs in the fabrication of low loss HCFs.

V Acknowledgements

We gratefully acknowledge support from Innovate UK (project 103973), EPSRC Programme grant Airguide (EP/P030181/1), the Royal Society, and the Royal Academy of Engineering. We also thank Mark Mason and Adrian Potasnik for assistance with fiber rewinding and technical support.

VI References

[1] Hodgkinson, J. and Tatam, R. P., "Optical gas sensing: a review," Meas. Sci. Technol. 24, 012004, 1-59 (2013).

[2] Jin, W., Ho, H.L., Cao, Y.C., Ju, J. and Qi, L.F., "Gas detection with micro- and nano- engineered optical fibers," *Optical Fiber Technology*, **19**(6) B, 741-759 (2013).

[3] Hanf, S., Keiner, R., Yan, D., Popp, J. and Frosch, T., "Fiber-Enhanced Raman Multigas Spectroscopy: A Versatile Tool for Environmental Gas Sensing and Breath Analysis," *Analytical Chemistry* **86**(11), 5278–5285 (2014).

[4] Moseley, P.J., Huang, W.C., Welch, M.G., Mangan, B.J., Wadsworth, W.J. and Knight, J.C., "Ultrashort pulse compression and delivery in a hollow-core photonic crystal fiber at 540nm wavelength," *Optics Letters*, 35(21) 3589-3591 (2010).

[5] Chen, Y., Wheeler, N. V., Baddela, N. K., et al., "Understanding Wavelength Scaling in 19-Cell Core hollow-core photonic bandgap fibers," *Proc. Optical Fiber Communication Conference*, OSA Technical Digest (online) (Optical Society of America, 2014), M2F.4 (2014).

[6] Bradley, T. D., Hayes, J. R., Chen, Y., et al., "Record low-loss 1.3 dB/km data transmitting antiresonant hollow core fibre," *Proc. Eur. Conf. on Optical Communication*, PDP Th3F.2, (2018).

[7] Chafer, M., Delahaye, F., Amrani, F., Debord, B., Gerome, F. and Benabid, F., "1 km long HC-PCF with losses at the fundamental Rayleigh scattering limit in the green wavelength range," *Conference on Lasers and Electro-Optics (CLEO) 2018*, SF1K.3, (2018).

[8] Gao, S.-F., Wang Y. Y., Ding W., Hong Y. F., and Wang P., "Hollow-Core Conjoined-Tube Negative-Curvature Fiber with Loss approaching Rayleigh Scattering Limit of Silica." In *CLEO: Science and Innovations*, pp. STh1L-6. Optical Society of America (2019).

[9] Hayes, J R., Sandoghchi, S.R., Bradley, T.D., Liu, Z., Slavík, R., Alonso Gouveia, M., Wheeler, N.V. et al. "Antiresonant hollow core fiber with an octave spanning bandwidth for short haul data communications." *Journal of Lightwave Technology* 35(3), 437-442 (2017)

[10] Dicaire, I., Beugnot, J.C. and Thevenaz, L., "Analytical modeling of the gas-filling dynamics in photonic crystal fibers," *Applied Optics*, **49**(24) 4604- 3609, (2010).

[11] Jasion, G.T., Hayes, J.R., Wheeler, N.V., Chen, Y., Bradley, T.D., Richardson, D.J., and Poletti, F., "Fabrication of tubular anti-resonant hollow core fibers: modelling, draw dynamics and process optimization," Opt. Express 27, 20567-20582 (2019)

[12] Gao, S., Wang, Y.Y., Liu, X-L., Hong, C., Gu, S. and Wang, P., "Nodeless Hollow-Core Fiber for Visible Spectral Range," *Optics Letters*, **42**(1) 61-64 (2017).

[13] Fokoua, E. N., Chen, Y., Richardson, D. J., & Poletti, F., "Microbending effects in hollow-core photonic bandgap fibers". In *ECOC 2016; 42nd European Conference on Optical Communication* (pp. 1-3). VDE (2016).

[14] Sakr, H., Bradley, T. D., Hong, Y., Jasion, G. T., et al. "Ultrawide Bandwidth Hollow Core Fiber for Interband Short Reach Data Transmission" In *Optical Fiber Communication Conference* (pp. Th4A-1). Optical Society of America (2019)